Re-Os SYSTEMATICS OF LÖLLINGITE AND ARSENOPYRITE IN GRANULITE FACIES GARNET ROCKS: INSIGHTS INTO THE METAMORPHIC HISTORY AND THERMAL EVOLUTION OF THE BROKEN HILL BLOCK DURING THE EARLY MESOPROTEROZOIC (NEW SOUTH WALES, AUSTRALIA)

N. J. Saintilan

Department of Earth and Atmospheric Sciences, University of Alberta, Edmonton, Alberta, T6G 2E3, Canada

R. A. Creaser

Department of Earth and Atmospheric Sciences, University of Alberta, Edmonton, Alberta, T6G 2E3, Canada

P. G. Spry

Department of Geological and Atmospheric Sciences, 253 Science I, Iowa State University, Ames, Iowa, 50011-3212, USA

D. Hnatyshin

Department of Earth and Atmospheric Sciences, University of Alberta, Edmonton, Alberta, T6G 2E3, Canada

Corresponding author:
Nicolas J. Saintilan
saintila@ualberta.ca

Abstract

Löllingite and arsenopyrite aggregates occur in spessartine-almandine garnet rocks (garnetite) metamorphosed to granulite facies, which are spatially associated with Pb-Zn-Ag mineralization in the supergiant Broken Hill deposit, southern Curnamona Province (SCP), New South Wales, Australia. Sulfides/sulfarsenides comprise löllingite and coexisting arsenopyrite ± galena ± tetrahedrite that occur interstitial to garnet crystals. Löllingite formed first while gold-bearing löllingite, which occurs as rare relicts in arsenopyrite, was destroyed to produce arsenopyrite ± detectable micro-inclusions of invisible gold.

Standard mineral separation procedures produced pure separates of löllingite, arsenopyrite, and mixtures of arsenopyrite ± löllingite and löllingite ± arsenopyrite. In a plot of $^{187}Re/^{188}Os$ vs. $^{187}Os/^{188}Os$ samples of löllingite and löllingite ± arsenopyrite have $^{187}Re/^{188}Os$ ratios between 6.87 and 7.40 and $^{187}Os/^{188}Os$ ratios between 0.8506 and 0.8651, whereas arsenopyrite and arsenopyrite ± löllingite samples have higher $^{187}Re/^{188}Os$ ratios (7.14 to 11.32) and more radiogenic $^{187}Os/^{188}Os$ ratios (0.8828 to 0.9654). Thirteen analyses of arsenopyrite and arsenopyrite ± löllingite define a Model 1 isochron with an age of 1574 ± 38 Ma (2σ; MSWD = 1.4, initial $^{187}Os/^{188}Os$ ratio of 0.666 ± 0.006), whereas the five löllingite and löllingite ± arsenopyrite samples define a Model 1 isochron with an age of 1707 ± 290 Ma (2σ; MSWD = 0.32, initial $^{187}Os/^{188}Os$ ratio [Os]i = 0.652 ± 0.036) that is indistinguishable from the arsenopyrite age. Re and Os contents are extremely high for löllingite and arsenopyrite (Re = 120–475 ppb; Os = 65–345 ppb) likely as a result of concentration of Re and Os in these minerals during granulite facies metamorphism from the inferred exhalite protolith. Petrographic observations combined with the Model 1 Re-Os ages and literature SHRIMP U-Pb ages of monazite in garnetite suggest that arsenopyrite formed on the retrograde path at the expense of löllingite.

Cooling from peak Olarian *P–T* conditions (~800 °C at 1602 Ma) to at least 550 °C (first temperature of stability of arsenopyrite) at ca. 1574 Ma occurred at a rate of ~9 °C Myr^{-1}, which is similar to the rate of cooling determined for previously published SHRIMP U-Pb ages from successive monazite generations (McFarlane and Frost, 2009). These results are consistent with the late phase of retrograde metamorphism that was initiated between ca. 1590 and 1575 Ma.

Introduction

Safflorite ($CoAs_2$), rammelsbergite ($NiAs_2$) and löllingite ($FeAs_2$) form a solid solution series with estimated crystallization temperatures for these minerals between 550 and 625 °C (Raič et al., 2014). Löllingite occurs in high-grade metamorphosed (i.e., amphibolite to granulite facies) sulfide deposits where it typically forms at the expense of arsenopyrite (FeAsS) through a loss of volatiles (e.g., H_2S) during prograde metamorphism (Tomkins and Mavrogenes, 2001; Davies et al., 2010). In pyrite-poor massive sulfide deposits containing disseminated iron silicates or oxides, metamorphic processes lower $f(S_2)$ and promote the solid-state conversion of arsenopyrite to löllingite and pyrrhotite, rather than arsenopyrite melting (Pokrovski et al., 2002; Tomkins et al., 2006). Arsenopyrite may form at the expense of löllingite through addition of volatile (e.g., H_2S) and cooling during retrograde metamorphism (e.g., Tomkins and Mavrogenes, 2001).

Occurrences of disseminated löllingite and arsenopyrite crystals (hereafter referred to as "sulfarsenides") are reported in spessartine-almandine garnet rocks or "garnetite" metamorphosed to the granulite facies that are spatially associated with the Broken Hill Pb-Zn-Ag deposit, New South Wales, Australia (Fig. 1; Spry and Wonder, 1989; Plimer, 2006). Petrographic work by Spry (1978) and Plimer (2006) suggested that arsenopyrite in garnetite is the product of the breakdown of pre-existing löllingite during retrograde metamorphism.

The present work aims to determine an age for the sulfarsenides in garnetite using the Re-Os isotope system and processing individual löllingite and arsenopyrite mineral separates. In an ideal case, distinct Re-Os ages for the prograde phase (precipitation of löllingite) and retrograde phase (precipitation of arsenopyrite) might be determined, and allow us to evaluate the conclusions of Spry (1978) and Plimer (2006) regarding the timing of formation of these minerals. In addition, by combining literature data on the temperature of precipitation and stability fields of löllingite and arsenopyrite with the obtained Re-Os ages, we may bring new insights into the metamorphic and thermal evolution (cooling rate?) of the Broken Hill block. The Re-Os data are compared to data obtained previously using the U-Th-Pb geochronometer in zircon and monazite, Sm-Nd geochronometer of garnet, and the Ar-Ar ages of hornblende, plagioclase and clinopyroxene for the tectono-metamorphic and thermal events that affected garnetite and other Mesoproterozoic to Cambrian metamorphic rocks in the Broken Hill area (e.g., Harrison and McDougall, 1981; Ehlers et al., 1996; Page et al., 2005a, b).

Geological background

The Broken Hill ore deposit occurs in metasedimentary rocks of the Paleoproterozoic Willyama Supergroup, which lie within the fault-bounded Broken Hill Domain of the Curnamona Craton (Fig. 1b). SHRIMP U-Pb geochronology using zircon constrains the age of the Willyama Supergroup at 1686 ± 3 Ma to 1689 ± 5 Ma (1σ, Page et al., 2005a, b), which is conformably overlain by the Sundown Group that is younger than 1672 ± 7 Ma (Page et al., 2005a). The Broken Hill Domain is characterized by a regional prograde metamorphic pattern with amphibolite facies in the NW to granulite facies in the SE (Binns, 1964; Phillips, 1980; Phillips and Wall, 1981). The Willyama Supergroup was subjected to at least three phases of deformation (D_1-D_3) associated with the Olarian Orogeny between ~1575 to 1657 Ma (e.g., Page and Laing, 1992; Page et al., 2005a, b; Forbes et al., 2008; McFarlane and Frost, 2009). Folds

96 associated with these deformation events are isoclinal (D_1), macroscopic tight with near vertical axial
97 planes (D_2), and near-vertical open with D_3 (Laing et al., 1978). U-Pb zircon ages for D_2 and D_3 are
98 indistinguishable and dated within the interval 1597 ± 3 to 1591± 5 Ma (zircon; Page et al., 2005a). Due to
99 complexities of structural interpretation a specific age for D_1 is uncertain although it likely overlapped the
100 older 1597 ± 3 Ma age given for the age interval for D_2-D_3 (Page et al., 2005a). Metamorphic conditions
101 are slightly higher for D_1 than D_2 (Majoribanks et al., 1980; Frost et al., 2005) with peak conditions of
102 ~780°C and ~5.2 kbar (Phillips, 1980; Phillips and Wall 1981) affecting the Broken Hill deposit.
103 Retrograde metamorphism (T = 550 to 600 °C, P = 5 to 5.5 kbar; Phillips, 1980; Corbett and Phillips,
104 1981; Stevens, 1986) began during D_3 and is associated with initiation of retrograde shear zones that occur
105 throughout the Broken Hill area and crosscut the Broken Hill deposit. This retrograde history is supported
106 by ^{40}Ar-^{39}Ar cooling ages (hornblende, clinopyroxene, muscovite) in the range of 1550 to 1500 Ma
107 suggesting that the area cooled down to and below 500 °C at a rate of ~3 °C Myr^{-1} between 1660 Ma and
108 1570 Ma (Harrison and McDougall, 1981). Following granitoid emplacement at c. 1500 Ma, the region
109 remained below 350°C until a thermal event affected the Curnamona Province during the Delamerian
110 orogeny in early Paleozoic time (Harrison and McDougall, 1981). Retrograde regional shear zones in
111 Paleoproterozoic basement rocks of the Curnamona Province comprise greenschist- to amphibolite-grade
112 mineral assemblages that formed between 517 and 497 Ma (Dutch et al., 2005). The P-T conditions
113 calculated from the garnet-staurolite-biotite-muscovite-chlorite-quartz-bearing mineral assemblages in the
114 shear fabrics are between 530 and 600 °C at ca. 5 kbar (Dutch et al., 2005) whereas Harrison and
115 McDougall (1981) suggested that temperatures only locally reached ~350 °C at 520 ± 40 Ma (Rb-Sr,
116 biotite; ^{40}Ar-^{39}Ar, plagioclase).
117 The Broken Hill ore deposit within the Broken Hill domain comprises six stacked orebodies that
118 were metamorphosed to the granulite facies and affected by large, recumbent, isoclinal D_2 folds (Fig. 1c;

Plimer, 2006). The orebodies are spatially associated with three types of garnet-rich rock (quartz garnetite, garnetite, and so-called "garnet envelope"), which are described in detail by Spry and Wonder (1989), Plimer (2006), and Spry et al. (2007) and are not repeated here (Figs. 1c-d). Although it should be noted that garnet envelope occurs on the margins of the Pb-rich orebodies as garnet stringers discordant to S_0 and S_1, generally parallel to S_3, or where garnet t surrounds veins that cross-cut quartz garnetite (Spry and Wonder, 1989). Garnetite contains > 80% of garnet along with various accessory minerals (e.g., quartz, plagioclase, gahnite, sulfides, sulfosalts, arsenides, sulfarsenides) that were tabulated in Spry and Wonder (1989, their Table 2). In places, blue quartz-bearing garnetite contains euhedral to subhedral arsenopyrite up to 0.5 cm in length (Fig. 2a). Garnetite occurs mostly on the margins of lenses 1, 2, and 3 and the A lode, as inclusions in mineralization, and along strike from sulfide mineralization. Plimer (2006) and Spry et al. (2007) describe laminations in garnetite that mainly parallel bedding and the S_1 schistosity (the axial plane schistosity of F_1 folds). However, in places, garnetite is chaotically folded and unrelated to S_1. The origin of garnetite is controversial and is centred on three main proposals: (1) metamorphism of manganiferous sediments (e.g., Wright et al. 1987; Spry and Wonder, 1989; Lottermoser, 1989, Plimer, 2006; Spry et al. 2007); (2) metasomatic mobilisation of Mn between the sulfide lenses and the wall rocks either syn- (D_1-D_2) or post-peak metamorphism (D_3) (Hodgson, 1975; Prendergast et al., 1998); (3) reaction of Mn derived from partially melted sulfide orebodies with the surrounding pelitic gneisses (Frost et al., 2002; Sparks and Mavrogenes, 2003). It should be noted that Plimer (2006) proposed that garnetite formed as a result of possible retrograde metamorphic reactions fostered by the rheological contrast between galena-rich sulfide orebodies and the enclosing metamorphic silicate rocks. Preliminary U-Pb zircon ages and Sm-Nd garnet ages in garnetite yielded "a metamorphic age of around 1590 Ma" (Ehlers et al., 1996). Regardless of the origin of garnetite, it is clear that it is a metamorphic rock that was

subjected to granulite facies metamorphism during the Olarian orogeny and to a Cambrian thermal event during the Delamarian orogeny.

Methodology

Relationships between arsenopyrite and löllingite were studied by means of optical and scanning-electron microscope (SEM) on a representative polished thin section from a garnetite sample "532-35", containing arsenopyrite (Fig. 2a and b), located between the 1 and 2 lenses on the 21 level of the old New Broken Hill Consolidated mine at the southern end of the Broken Hill deposit. A Zeiss Sigma 300 Field Emission SEM (VP-FESEM) was operated in backscattered electron mode (SEM-BSE, beam conditions of 15kV). A Bruker energy dispersive X-ray spectroscopy (EDS) system with dual silicon drift detectors each with an area of 60 mm^2 and a resolution of 123 eV was used for single spot analysis.

Sample 532-35 was cut into slabs that were thoroughly cleaned using silicon carbide grit and paper to remove any metal traces left by hammering or sawing. The sample was crushed using agate mortar and pestle and sieved through disposable home-made nylon sieves to produce 70–200 and +70 mesh size fractions. These fractions were treated by standard heavy liquid separation and arsenopyrite and löllingite were extracted by magnetic concentration using a Frantz Isodynamic Separator to produce magnetic (M) and non-magnetic (NM) fractions by applying successive 1.7 and 2.2 amp currents with 15 ° side slope and 10 ° forward slope, and, 2 ° side slope and 10 ° forward slope for these currents respectively. A fraction is thus always referred to as follows: "mesh size, magnetic property, and side slope/forward slope". The composition of each mineral separate was determined by X-ray diffraction (XRD) analyses and visually assessed by SEM-BSE images complemented by qualitative SEM-EDX analysis (Table 1).

For each Re-Os analysis, between 12 and 36 mg of arsenopyrite or löllingite mineral separates were weighed and transferred into thick-walled borosilicate Carius tubes. Each sample was dissolved in inverse aqua regia (~2mL of 10 N HCl and ~6 mL 16 N HNO_3) with a known amount of ^{185}Re+^{190}Os spike solution at 220 ºC for 24 hours. The full Re-Os laboratory protocol used in the present study is given in Hnatyshin et al. (2016). Rhenium and Os isotopic compositions were determined by negative thermal ionisation mass spectrometry (NTIMS; Creaser et al., 1991; Völkening et al., 1991) using a ThermoScientific Triton mass spectrometer at the Canadian Centre for Isotopic Microanalysis, University of Alberta, Edmonton, Canada. Rhenium was measured as ReO_4^- in static mode on Faraday collectors, whereas Os was measured as OsO_3^- in peak-hopping mode on SEM with a constant flow of oxygen (Creaser et al., 1991; Völkening et al., 1991).Total procedural blanks returned the following values (Batch #1, n = 3 procedural blanks, for samples UA-01-BHA to UA-14-BHA, Re = 4.4 ± 0.98 pg (1σ), Os = 1.34 ± 0.03 pg (1σ), blank $^{187}Os/^{188}Os$ = 0.27; Batch#2 for samples UA-15-BHA to UA-18-BHA, Re = 2.3 ± 0.47 pg (1σ), Os = 0.08 ± 0.05 pg (1σ), blank $^{187}Os/^{188}Os$ = 0.80). Measurement quality was monitored by repeated measurements of in-house Re (natural Re, $^{185}Re/^{187}Re$ = 0.59774 ± 0.00065, n = 23) and Os (AB-2, $^{187}Os/^{188}Os$ = 0.10682 ± 0.00009, n = 100) standard solutions. Rhenium analyses are corrected for isobaric oxide interferences, and normalized to a value of 0.5974 based on the long-term measurements of the Re standard. Raw OsO_3^- ratios are corrected for isobaric oxides interferences, spike contribution and mass fractionation using a $^{192}Os/^{188}Os$ value of 3.08261 using an exponential law (Hnatyshin et al., 2016). Isochron regression of the Re-Os data was performed using Isoplot v 4.15 (Ludwig, 2011) using the ^{187}Re constant of Smoliar et al. (1996).

Results

Petrography

In hand specimen, aggregates of arsenopyrite and löllingite occur interstitially to garnets (Figs. 2a and b). Arsenopyrite occurs locally as euhedral crystals up to 0.5 cm in diameter (Figs. 2a and b), but it also occurs as dissemination along with löllingite throughout the rock as anhedral aggregates. Each aggregate shows a core of black löllingite that is irregularly rimmed by grey arsenopyrite (Fig. 2b). Galena is visible in hand specimen at the contact between these two phases.

SEM-BSE images show irregular contacts between löllingite and arsenopyrite and inclusions of löllingite in arsenopyrite (Fig. 2c, d and e). Fractures present in löllingite were filled in by tetrahedrite. These fractures are not visible in arsenopyrite and must predate its formation. Hence, löllingite ± tetrahedrite predates the formation of arsenopyrite (Fig. 2f). Galena formed after löllingite ± tetrahedrite, and as late rims on arsenopyrite or filling fractures in arsenopyrite. In some rare instances, small inclusions (< 10 μm) of arsenopyrite occur in löllingite and might indicate that arsenopyrite was present prior to löllingite precipitation. Alternatively, these inclusions might be local replacement of löllingite by arsenopyrite as it appears to be the most common texture in the studied sample.

These petrographic observations were complemented by SEM-EDX analyses of löllingite and arsenopyrite (average values in Table 1, full data set available as Electronic Supplementary Material 1). In sample 532-25, qualitative analyses of löllingite shows that it contains an average of 4.0 wt % Co, 2.0 wt. % Ni, and 1.3 wt% S, whereas arsenopyrite contains lower amounts of Co (~2.1 wt. %) and Ni (~0.1 wt. %). Unobservable but detectable gold, which is referred to as "invisible gold" (cf. Tomkins and Mavrogenes, 2001), was identified through single spot SEM-EDX analyses as disseminated micro-inclusions in arsenopyrite (e.g., Figs. 2c and e, Point A = 2.0 wt% Au; Fig. 2e, Point B = 4.8 wt% Au).

Mineral separates and XRD data

Five magnetic and non-magnetic fractions were obtained during sample processing (Table 2). All fractions correspond to sulfarsenides with trace amounts of galena or tetrahedrite as verified by XRD analyses. The purity of these mineral fractions was assessed by means of SEM-BSE images and XRD analyses (Fig. 3). Three fractions correspond to 100% pure monomineral fractions of arsenopyrite or löllingite: (1) "70-200, NM 2.2, 2/10" and "+70, NM 2.2, 2/10" fractions containing arsenopyrite (Fig. 3a), (2) "70-200, M 1.7, 15/10" fraction containing cobaltian löllingite (Fig. 3b). The two remaining fractions correspond to mixtures of these sulfarsenides in different proportions: (1) "+70, M 1.7, 15/10" fraction corresponds to 80–100% löllingite and 0–20% arsenopyrite (Fig. 3c), (2) "+70, M 2.2., 2/10" fraction corresponds to 70–100% arsenopyrite and 0–30% löllingite (Fig. 3d).

Re-Os isotope geochemistry

The results of 18 Re-Os isotope analyses of the sulfarsenide mineral separates are presented in Table 2. These data reveal high Re contents systematically higher than 120 ppb in both löllingite and arsenopyrite and two overlapping ranges of Re contents depending on the type of sulfarsenide mineral: (1) between 120 and 385 ppb Re in arsenopyrite, (2) between 300 and 475 ppb Re in löllingite. Osmium concentrations are also very high (>63 ppb) in these sulfarsenides. The löllingite and löllingite ± arsenopyrite samples have the highest total Os contents (222 to 346 ppb), whereas arsenopyrite and arsenopyrite ± löllingite samples have lower total Os contents (64 to 255 ppb). Uncertainties (±2σ) are 0.36% or better for Re abundances and 0.26% or better for Os. The variation in total Re (and corresponding radiogenic ^{187}Os*) and common ^{192}Os contents between the sulfarsenide minerals resulted in a relatively narrow range of low ^{187}Re/^{188}Os and low radiogenic ^{187}Os/^{188}Os ratios. Löllingite and löllingite ± arsenopyrite samples plot in the bottom left-hand corner of the ^{187}Re/^{188}Os vs. ^{187}Os/^{188}Os plot with ^{187}Re/^{188}Os ratios between 6.87 and 7.40 and ^{187}Os/^{188}Os ratios between 0.8506 and 0.8651, whereas

arsenopyrite and arsenopyrite ± löllingite samples have higher $^{187}Re/^{188}Os$ ratios (7.14 to 11.32), and more radiogenic $^{187}Os/^{188}Os$ ratios (0.8828 to 0.9654; Fig. 4a).

On a conventional $^{187}Re/^{188}Os$ vs. $^{187}Os/^{188}Os$ plot, the 13 arsenopyrite and arsenopyrite ± löllingite samples define a Model 1 isochron with an age of 1574 ± 38 Ma (Fig. 4b; 2σ; mean squared weighted deviates, MSWD = 1.4, initial $^{187}Os/^{188}Os$ ratio [Os]i = 0.666 ± 0.006). Despite the small range of $^{187}Re/^{188}Os$ ratios (~7 to ~12), the fit of data to the regression line yields a 2σ age uncertainty of only +/- 2.4%. The 5 löllingite and löllingite ± arsenopyrite samples define a Model 1 isochron with an age of 1707 ± 290 Ma (Fig. 4c; 2σ; mean squared weighted deviates, MSWD = 0.32, initial $^{187}Os/^{188}Os$ ratio [Os]i = 0.652 ± 0.036). Given the narrow spread of $^{187}Re/^{188}Os$ ratios (~6.8 to ~7.8), the fit of data to the regression line yields a large 2σ age uncertainty of ~17%. This age and its original Os ratio overlap within error with the age and original Os ratio defined by the arsenopyrite samples.

Discussion

Relative chronology between löllingite and arsenopyrite and invisible gold in arsenopyrite

Our petrographic observations of irregular contacts between löllingite and arsenopyrite and relicts of löllingite in arsenopyrite crystals (Figs. 2c, d, and e) are similar to the textures observed by Tomkins and Mavrogenes (2001; their figure 5c) for the formation of arsenopyrite at the expense of löllingite during retrograde metamorphism (Fig. 2f). Consequently, arsenopyrite and löllingite are in petrographic disequilibrium. Tomkins and Mavrogenes (2001) suggested that this texture is also diagnostic of the original complete prograde metamorphism of arsenopyrite to löllingite. The only evidence in favor of this interpretation in our case are the rare blebs of arsenopyrite (< 10μm) that are tentatively interpreted as relicts of arsenopyrite that were metamorphosed during a prograde phase.

252 The destruction of löllingite during retrograde metamorphism would explain the presence of trace Co
253 and Ni and their uneven distribution in arsenopyrite (Table 1). In addition, the detection of invisible gold
254 in arsenopyrite is a feature that can be explained by the destruction of löllingite and the redistribution of
255 gold during retrograde metamorphism (cf. Tomkins and Mavrogenes, 2001). Indeed, desulfidation of a
256 gold-sulfur complex under metamorphic conditions lower than granulite facies could result in the co-
257 precipitation of arsenopyrite, löllingite, pyrrhotite and native gold. In addition, arsenopyrite, löllingite and
258 pyrrhotite would not necessarily be in close spatial association. In the current study, the absence of
259 pyrrhotite in the observed sulfarsenide aggregates, the relicts of löllingite in arsenopyrite, and the presence
260 of native gold disseminated in arsenopyrite are favourable arguments to support the mechanism presented
261 for post-peak metamorphic gold presence in arsenopyrite by Tomkins and Mavrogenes (2001). This
262 conclusion is supported further by the Re-Os absolute Re-Os age determination interpreted in the
263 following section.
264
265 *Significance of the Re-Os age in sulfarsenides and insights into the thermal evolution of the Broken Hill*
266 *area during the Early Mesoproterozoic*
267 The Re-Os age of 1574 ± 38 Ma recorded by the Re-Os isotopic system in arsenopyrite, represents
268 time at which the Re-Os isotopic system was closed in arsenopyrite. The imprecise age recorded by the
269 Re-Os isotopic system in löllingite overlaps within error with the age defined by the arsenopyrite data
270 points. Our petrographic observations show that löllingite and arsenopyrite are in petrographic
271 disequilibrium but the Re-Os isotope data are not sufficient to determine when löllingite formed prior its
272 partial destruction to arsenopyrite during retrograde metamorphism at ca. 1574 Ma. Indeed, according to
273 the summary of known metamorphic and thermal events that affected the Broken Hill Block in the
274 Curnamona Craton (Table 3), the Re-Os age of arsenopyrite indicates that it formed during retrograde

metamorphism affecting the garnetite that is proposed to have started from ca. 1590 to 1575 Ma (cf. McFarlane and Frost, 2009). Our isotope geochemistry results are consistent with the interpretation of Spry (1978) who had determined that the cores of arsenopyrite, where intergrown with pyrrhotite, have high As:S ratios relative to the rims. He concluded that this pattern was diagnostic of growth of arsenopyrite during retrograde metamorphism, as based on the studies of Kretschmar and Scott (1976) and Sharp et al. (1985).

McFarlane and Frost (2009) proposed that the SHRIMP ca. 1575 Ma age recorded in their youngest monazite grains corresponds to the timing of final cooling of the rocks of the Broken Hill Block below minimum granitic melt temperatures of ca. 650 °C at a rate of ~10 °C Myr^{-1}. According to the experiments of Sharp et al. (1985), the use of the arsenopyrite geothermometer in our Broken Hill sample is precluded because this geothermometer yields an underestimation of the actual temperature of mineral precipitation for deposits metamorphosed to upper amphibolite and granulite facies. This underestimation is even more significant considering the trace element contents of arsenopyrite in our sample (2.1 wt% Co and 0.1 wt% Ni in arsenopyrite, EDX analyses, this study; arsenopyrite containing up to 3.19 wt. % Co, 0.49 wt. % Ni, n = 51, microprobe analyses by Spry, 1978). However, given the fact that arsenopyrite is stable at temperatures in the range of 400 to 550 °C (Pokrovski et al., 2002; Tomkins et al., 2006; Raič et al., 2014), we may use 550 °C as the minimum temperature for the precipitation of arsenopyrite. Thus, cooling from peak Olarian *P–T* conditions (~800 °C at 1602 Ma; McFarlane and Frost, 2009) to at least 550 °C at ca. 1574 Ma occurred at a rate of ~9 °C Myr^{-1}, i.e., a similar value that determined by McFarlane and Frost (2009) using SHRIMP U-Pb ages of successive monazite generations. These results are also consistent with the timing of the closure of the Sm-Nd system in metamorphic garnet (600 ± 30 °C; Mezger et al., 1992) that occurred at 1580 Ma (Hand et al., 2003).

297 Löllingite forms at temperatures between 625 and 550 °C, whereas the destruction of löllingite to
298 form arsenopyrite occurs when temperature goes below 550 °C and enters the stability field of
299 arsenopyrite (Pokrovski et al., 2002; Tomkins et al., 2006; Raič et al., 2014). Tomkins and Mavrogenes
300 (2002) reported pre- to syn-peak metamorphic conditions in granulite-hosted gold deposits (e.g.,
301 Challenger and Griffin Find) in which löllingite survived temperatures of 700 to 850 °C and pressures of
302 ~6 to 7.5 ~kbars. Considering the thermal constraints presented above for the retrograde cooling path for
303 Broken Hill and the summary of events for both the prograde and retrograde paths in Table 3, our Re-Os
304 age of 1707 ± 290 Ma suggests two possible scenarios for the formation of löllingite: (1) between ca. 1657
305 Ma and ca. 1630 Ma when T was between 550 and 650°C prior to peak metamorphic conditions of ~800
306 °C at ca. 1602 Ma, or alternatively, (2) after ca. 1580 Ma when temperatures went below 600 ± 30 °C. At
307 the current state of knowledge, we cannot choose between either of these hypotheses.
308
309 *Regional implications and evolution of the Broken Hill area compared to the Mount Isa Block during the*
310 *Early Mesoproterozoic*
311 Stratigraphic rationalization and SHRIMP U-Pb geochronology carried out in the eastern Mount
312 Isa Block and the Curnamona Province, in complement to the original lithologic, metamorphic and
313 metallogenic similarities recognized in these terranes (Vaughan and Stanton, 1984; Laing and
314 Beardsmore, 1986), support a strong correlation over the interval ca. 1710 to 1580 Ma between these
315 terranes from deposition of the Willyama Supergroup (Curnamona Province) and Maronan Supergroup
316 (eastern Mount Isa Block) to the initial stages of the Olarian (Curnamona Province) and Isan (eastern
317 Mount Isa Block) orogenies (Giles et al., 2004). These authors included the Mount Isa block and the
318 Curnamona Province within the same ca. 1600 to 1500 Ma orogenic belt (cf. their Figure 4) and a late
319 phase of thick-skinned deformation and crustal shortening was identified for the Isan orogeny at ca. 1550

to 1500 Ma (MacCready et al., 1998). In particular, two metamorphic events, which affected the Western Fold Belt of the Mount Isa Inlier, were identified at ca. 1575 Ma (Hand and Rubatto, 2002), and 1532 ± 7 Ma, the latter of which was associated with the emplacement of pegmatite (Connors and Page, 1995). Our Re-Os age of ca. 1574 Ma for the formation of arsenopyrite in garnetite during retrograde metamorphism in the Curnamona Province adds evidence for coeval metamorphic events recorded in the Western Fold Belt of the Mount Isa Inlier and the Curnamona Province on the retrograde path.

Apparent closure temperatures of the Re-Os isotopic system in arsenopyrite

The blocking temperature of an isotope geochronometer in a given mineral species is a measure of its ability to retain primary age information through geologic and thermodynamic events. A minimum apparent closure temperature for the Re-Os arsenopyrite chronometer was conservatively estimated at 400 °C with the possibility of exceeding 450 °C (Morelli et al., 2010).

The only dynamothermal event that may have affected the arsenopyrite-löllingite-bearing garnetite rocks at Broken Hill is a Delamerian event with (1) temperatures of 530 to 600 °C localized in regional shear zones at 517 to 497 Ma (Dutch et al., 2005), and, (2) a regional gradient up to ~350 °C at ca. 520 Ma (Harrison and McDougall, 1981). Our Re-Os age of arsenopyrite corroborates petrographic observations in favor of arsenopyrite precipitation during retrograde metamorphism. This is consistent with closure of the Re-Os isotopic system during the Early Mesoproterozoic and its subsequent preservation once arsenopyrite had precipitated. Given that our garnetite sample was collected away from any Delamerian-age shear zones, our results imply that the Re-Os isotopic system was not disturbed by the ~350 °C Delamerian regional event. Our data confirm the proposal by Davies et al. (2010) and Morelli et al. (2010) for an estimate of closure temperature of the Re-Os isotopic system of ca. 400 to possibly 450 °C in arsenopyrite, i.e., the lower stability limit of arsenopyrite (400 to 550 °C; Pokrovski et al., 2002;

343 Tomkins et al., 2006). By corollary, the preservation of the yet imprecise Re-Os age in löllingite (stability
344 field of 625 to 550 ºC) indicates that this Delamerian thermal event was not sufficient to reset the Re-Os
345 isotopic system in löllingite either. In conclusion, our study supports the findings of Davies et al. (2010)
346 and Morelli et al. (2010) that the potential for Re-Os dating in arsenopyrite and löllingite in high-grade
347 metamorphic rocks is high, since the Re-Os systematics for these minerals appear not to be to readily
348 disturbed by a later thermal event.
349
350 *Rhenium concentrations in arsenopyrite and löllingite, possible source of Re, and Re-Os evidence on the*
351 *origin of the Broken Hill deposit*

352 Our Re-Os isotope study shows that löllingite can contain high proportions of Re (>320 ppb) and
353 Os (> 220,000 ppt) that are unusual for metallic minerals other than molybdenite (Freydier et al., 1997;
354 Lambert et al., 1998; Stein et al., 1998; Ruiz and Mathur, 1999; Mathur et al., 2000; Frick et al., 2001).
355 Such Re and Os contents are particularly unusual in sediment-hosted ore systems (Tristá-Aguilera et al.,
356 2006; Schneider et al., 2007) with the two following exceptions: (1) sulfides in the Ruby Creek Cu
357 deposit, Alaska, USA (e.g., Re in pyrite 525–2355 ppb, Re in chalcopyrite 80–3200 ppb, Re in bornite
358 1615–1700 ppb; Selby et al., 2009); (2) chalcopyrite and bornite from the Dzhezkazgan Cu deposit,
359 Kazakhstan (e.g., ; Re in chalcopyrite 3.3–9.4 ppm, Re in bornite 8–10 ppm; Box et al., 2012).
360 Arsenopyrite in the garnetite sample from Broken Hill has extremely high Re (120 to 380 ppb)
361 concentrations compared to the composition of arsenopyrite reported previously in the literature. For
362 example, arsenopyrite from the Homestake gold deposit, South Dakota, contains ~3.5–63 ppb Re (Morelli
363 et al., 2010), whereas that from the Three Bluffs gold deposit, Nunavut contains ~69–123 ppb Re (Davies
364 et al., 2010). In contrast to arsenopyrite from Homestake (total common Os contents of 3–21 ppt) and at
365 Three Bluffs (total common Os below 1.5 pg), for which the Os budget is almost exclusively composed of

^{187}Os, arsenopyrite at Broken Hill has total common Os contents in the range of 24 to 255 ppb, thus diluting the ^{187}Os budget. Common Os was thus available in the source protolith for incorporation in arsenopyrite, and, by corollary, in earlier-formed löllingite.

Our results and observations lead us to the following interpretations and hypotheses: (1) arsenides like löllingite are natural sinks for Re and Os, (2) arsenopyrite, which formed from the destruction of löllingite, has unusually high Re contents that were inherited like other trace elements (e.g., Co, Ni, see above) during the breakdown of Re-rich löllingite, (3) high Re contents in arsenide minerals such as löllingite might be explained by the fact that Re^{4+} forms diarsenides (e.g., similar to cubic sperrylite, $PtAs_2$) in which the oxidation state of arsenic is –2 (Szymanski, 1979).

If the assertion of Spry and Wonder (1989), Plimer (2006) and Spry et al. (2007) that garnetite is the product exhalite metamorphism is correct, then high concentrations of Re and Os in löllingite and arsenopyrite likely result from the concentration of Re and Os in these sulfarsenide minerals during metamorphism of the exhalite protolith. The initial $^{187}Os/^{188}Os$ ratio reflects the origin of bulk Os incorporated in a mineral at the time of precipitation prior to ingrowth of radiogenic ^{187}Os below the blocking temperature of the Re-Os system in this mineral (e.g., Walker et al., 1991). Löllingite and arsenopyrite have the same initial $^{187}Os/^{188}Os$ ratio of 0.66. Given that arsenopyrite formed at the expense of löllingite during retrograde metamorphism, this ratio reflects the origin of bulk Os incorporated in löllingite as it precipitated, and during conversion to arsenopyrite. Assuming that Os is sourced from exhalitive sediments that formed at about 1680 Ma (i.e., the age of the Willyama Supergroup; Page et al., 2005a), we can back calculate an estimate of the osmium isotopic composition of these sediments using the following equation (λ: decay constant of ^{187}Re; Smoliar et al., 1996; t = age of the Willyama Supergroup):

$$(^{187}Os/^{188}Os)_{sediments} = (^{187}Os/^{188}Os)_{sulfarsenides} - (^{187}Re/^{188}Os)_{sediments} * (e^{\lambda t} - 1).$$

If the exhalative sediments had a crustal $^{187}Re/^{188}Os$ signature of 34.5 (Peucker-Ehrenbrink and Jahn, 2001), our estimate of the $^{187}Os/^{188}Os$ ratio of these sediments at 1680 Ma would be 0.59. This estimate is much higher than what is expected for a mantle source ($^{187}Os/^{188}Os \sim 0.12$) suggesting the osmium source is, at least partially, of crustal origin. If the precursor to garnetite formed by the interaction of Mn-rich emanations from hydrothermal hot springs with pelagic clays (Spry and Wonder, 1989), the initial $^{187}Os/^{188}Os$ ratio may reflect an original geochemical composition of evolved upper continental crust with an overprint of seawater in hydrothermal springs. The initial ratio falls within the lower range of $^{187}Os/^{188}Os$ ratios proposed for the upper continental crust (cf., Saal et al., 1998) for which the accepted yet present-day estimates of Re concentrations are 0.2 to 2 ppb Re (Sun et al., 2003).

Conclusions

Garnetite spatially associated with the Broken Hill Pb-Zn-Ag deposit, which was metamorphosed to the granulite facies, contains aggregates of sulfarsenides that consist of arsenopyrite and löllingite ± galena ± tetrahedrite interstitial to garnet crystals. The conclusions of our Re-Os isotope geochemistry and petrographic study are:

- Aggregates of arsenic-rich minerals consist of a core of black löllingite surrounded by dull grey arsenopyrite that contain an unevenly distributed amount of Co, Ni, and invisible, but detectable, gold as a result of the breakdown of löllingite. Petrographic observations are consistent with the destruction of löllingite and the redistribution of gold during retrograde metamorphism, as proposed by Tomkins and Mavrogenes (2001) for several arsenopyrite-bearing gold deposits.
- Isochron regression of the Re-Os data points of arsenopyrite and arsenopyrite ± löllingite yields a Model 1 Re-Os age of 1574 ± 38 Ma (Early Mesoproterozoic). This age matches with the age of retrograde metamorphism (ca. 1590 to 1575 Ma) in the Broken Hill Block following peak

412 granulite facies metamorphism at ca. 1602 Ma, which is consistent with SHRIMP U-Pb ages of
413 monazite in garnetite (McFarlane and Frost, 2009). Isochron regression of the Re-Os data points
414 of löllingite and löllingite ± arsenopyrite yields an imprecise Model 1 age of 1707 ± 290 Ma that
415 overlaps within error with the age of arsenopyrite.

416 ● The arsenopyrite Re-Os age is consistent with an extended connection between the Olarian
417 orogeny in the Broken Hill Block and the Isan orogeny in the Mount Isa area for which two
418 distinct retrograde metamorphic events occurred at ca. 1575 Ma and ca. 1532 Ma.

419 ● Arsenopyrite and löllingite have unusually high concentrations of Re and Os for metallic minerals
420 other than molybdenite. An initial $^{187}Os/^{188}Os$ ratio of 0.66 determined through regression of Re-
421 Os data is common to the isochrons of löllingite data points on the one hand, and, arsenopyrite
422 ones on the other hand. This initial ratio is compatible with a calculated original ratio of 0.59 in
423 the sediments of the Willyaman Supergroup at ca. 1680 Ma, thereby indicating a, at least partially,
424 crustal source of Os. By corollary, considering that the garnetite formed with this initial
425 $^{187}Os/^{188}Os$ ratio may illustrate an original geochemical composition of an evolved upper
426 continental crust with overprint of seawater in hydrothermal springs; a scenario compatible with
427 the model of interaction of Mn-rich emanations from hydrothermal hot springs mixed with pelagic
428 clays in the long-lived Broken Hill Block (Spry and Wonder, 1989). It is proposed that Re
429 disseminated in the original Mn-rich exhalite protolith was concentrated in the sulfarsenide phases
430 during granulite facies metamorphism.

431 ● The Early Mesoproterozoic Re-Os age of arsenopyrite was retained despite a regional thermal
432 event (350 °C and ca. 5 kbar) at ca. 520 Ma during the Delamerian orogeny. Our study favors the
433 conservative estimate of 400 °C for the closure temperature of the Re-Os isotope system in
434 arsenopyrite (Davies et al., 2010; Morelli et al., 2010)

- The current study supports the conclusion of Davies et al. (2010) and Morelli et al. (2010) regarding the potential for Re-Os dating in arsenopyrite and löllingite that would have preserved original age information from high-grade metamorphic events, in particular in thermally long-lived Precambrian cratonic provinces.

Acknowledgements

This research was supported by the Swiss National Science Foundation (Swiss FNSNF) through an Early Postdoc.Mobility Grant (#P2GEP2_162075) awarded to N. J. Saintilan, and, an NSERC Discovery Grant awarded to R.A. Creaser. Mark Simms is thanked for assistance in mineral processing whereas Diane Caird ran XRD analyses at the University of Alberta. We thank Dr. Rafael del Rio and two anonymous reviewers for their detailed and pertinent reviews that contributed to greatly improve and clarify the manuscript. The work by Editor Dr. Lee Groat and Associate Editor Dr. Antoni Camprubi is acknowledged.

References

Binns, R.A. (1964) Zones of progressive regional metamorphism in the Willyama Complex, Broken Hill district, New South Wales. *J.Geol. Soc. Austral.***11**, 283-330.

Box, S.E., Syusyura, B., Seltmann, R., Creaser, R.A., Dolgopolova, A., and Zientek, M.L. (2012) Dzhezkazgan and associated sandstone copper deposits of the Chu-Sarysu basin, Central Kazakhstan. *Econ. Geol. Sp. Publ.* **16**, 303-328.

Connors, K.A., and Page, R.W. (1995) Relationships between magmatism, metamorphism and deformation in the western Mount Isa Inlier, Australia. *Prec. Res.* **71**, 131-153.

457 Corbett, G. J., and Phillips, G. N. (1981) Regional retrograde metamorphism of a high grade terrain: the
458 Willyama Complex, Broken Hill, Australia. *Lithos* **1**, 59-73.
459 Creaser, R.A., Papanastassiou, D.A., and Wasserburg, G.J. (1991) Negative thermal ion mass
460 spectrometry of osmium, rhenium and iridium. *Geochim. Cosmochim. Acta* **55**, 396-401.
461 Davies, T., Richards, J.P., Creaser, R.A., Heaman, L.M., Chacko, T., Simonetti, A., Williamson, J., and
462 McDonald, D.W. (2010) Paleoproterozoic age relationships in the Three Bluffs Archean iron
463 formation-hosted gold deposit, Committee Bay Greenstone Belt, Nunavut, Canada. *Explo. Mining*
464 *Geol.* **19**, 55-80.
465 Dutch, R.A., Hand, M., and Clark, C. (2005) Cambrian reworking of the southern Australian Proterozoic
466 Curnamona Province: constraints from regional shear-zone systems. *J. Geol. Soc. London* **162**, 763-
467 775.
468 Ehlers, K., Foster, J., Nutman, A.P., and Giles, D. (1996) New constraints on Broken Hill geology and
469 mineralisation. *In* New Developments in Broken Hill Type Deposits (J. Pongratz and G. Davidson,
470 eds.). *CODES Sp. Publ.***1**, 73-76
471 Forbes, C.J., Betts, P.G., Giles, D., and Weinberg, R. (2008) Reinterpretation of the tectonic context of
472 high-temperature metamorphism in the BrokenHill Block, NSW, and implications on the Palaeo- to
473 Meso-Proterozoic evolution. *Prec. Res.* **166**, p. 338–349.
474 Freydier, C., Ruiz, J., Chesley, J., McCandless, T. and Munizaga, F. (1997) Re-Os isotope systematic of
475 sulfides from felsic igneous rocks: Application to base metal porphyry mineralization in Chile.
476 *Geology* **25**, 775-778.
477 Frick, L.R., Lambert, D.D., and Hoatson, D.M. (2001) Re-Os dating of the Radio Hill Ni-Cu deposit, west
478 Pilbara craton, Western Australia. *Austral. J. Earth Sci.* **48**, 43-47.

Frost, B. R., Mavrogenes, J. A., and Tomkins, A. G. (2002) Partial melting of sulfide ore deposits during medium- and high-grade metamorphism. *Can. Mineral.* **40**, 1-18.

Frost, B.R., Swapp, S.M., and Gregory, R.W. (2005) Prolonged existence of sulfide melt in the Broken Hill orebody, New South Wales, Australia. *Can. Mineral.* **43**, 479-494.

Giles, D., Betts, P.G., and Lister G.S. (2004) 1.8-1.5 Ga links between the North and South Australian Cratons and the Early-Middle Proterozoic configuration of Australia. *Tectonophysics* **380**, 27-41.

Hand, M., and Rubatto, D. (2002) The scale of the thermal problem in the Mount Isa inlier. *Geol. Soc. Austral. Abs.* **67**, 173.

Hand, M., Rutherford, L., and Barovich, K. (2003) Garnet Sm-Nd age constraints on the timing of tectonism in the southwestern Curnamona Province: implications for existing models and correlations. *Geosc. Austral. Record* **13**, 65-68.

Harrison, T.M., and McDougall, I. (1981) Excess ^{40}Ar in metamorphic rocks from Broken Hill, New South Wales: implications for ^{40}Ar/^{39}Ar age spectra and the thermal history of the region. *Earth Planet. Sci. Lett.* **55**, 123-149.

Haydon, R.C., & McConachy, G.W. (1987) The stratigraphic setting of Pb-Zn-Ag mineralization at Broken Hill. *Econ. Geol.* **82**, 826-856.

Hnatyshin, D., Kontak, D.J., Turner, E.C., Creaser, R.A., Morden, R., and Stern, R.A. (2016) Geochronologic (Re-Os) and fluid-chemical constraints on the formation of the Mesoproterozoic-hosted Nanisivik Zn-Pb deposit, Nunavut, Canada: Evidence for early diagenetic, low-temperature conditions of formation. *Ore Geol. Rev.* **79**, 189-217.

Hodgson, C. J. (1975) The geology and geological development of the Broken Hill lode in the New Broken Hill Consolidated Mine, Australia. Part III: Petrology and petrogenesis. *J. Geol. Soc. Austral.* **22**, 195-214.

Kretschmar, U., and Scott, S.D. (1976) Phase relations involving arsenopyrite in the system Fe-As-S and their applications. *Can. Mineral.* **14**, 364-386.

Lambert, D.D., Foster, J.G., Frick, L.R., Hoatson, D.M., and Purvis, A.C. (1998) Application of the Re-Os isotopic system to the study of Precambrian sulfide deposits of Western Australia. *Austral. J. Earth Sci.* **45**, 265-284.

Laing, W.P., and Beardsmore, T.J. (1986) Stratigraphic rationalization of the Eastern Mount Isa Block, recognition of key correlations with Georgetown and Broken Hill Blocks in an eastern Australian Proterozoic terrain, and their metallogenic implications. *Geol. Soc. Austral. Abs.* **15**, 114-115.

Laing, W.P., Marjoribanks, R.W., and Rutland, R.W.R. (1978) Structure of the Broken Hill Mine area and its significance for the genesis of the orebodies. *Econ. Geol.* **73**, 1112-1136.

Lottermoser, B. G. (1989) Rare earth element study of exhalites within the Willyama Supergroup, Broken Hill Block, Australia. *Mineral. Deposita* **24**, 92-99.

Ludwig, K.R., 2011. User's manual for Isoplot 4.15: A geochronological toolkit for Microsoft Excel.

MacCready, T., Goleby, B.R., Goncharov, A., Drummond, B.J., and Lister, G.S. (1998) A framework of overprinting orogens based on interpretation of the Mount Isa deep seismic transect. *Econ. Geol.* **93**, 1422-1434.

Majoribanks, R.W., Rutland, R.W.R., Glen, R.A., and Laing, W.P. (1980) The structure and tectonic evolution of the Broken Hill region, Australia. *Prec. Res*. **13**, 209-240.

Mathur, R., Ruiz, J., and Munizaga, F., (2000) Relationship between copper tonnage of Chilean base-metal porphyry deposits and Os isotope ratios. *Geology* **28**, 555-558.

McFarlane, C.R.M., and Frost, B.R. (2009) Constraints on the early metamorphic evolution of Broken Hill, Australia, from in situ U-Pb dating and REE geochemistry of monazite. *J. Metam. Geol.* **27**, 3-17.

Mezger, K., Essene, E.J., and Halliday, A.N. (1992) Closure temperatures of the Sm-Nd system in metamorphic garnets. *Earth Planet. Sci. Lett.* **113**, 397-409.

Morelli, R.M., Bell, C.C., Creaser, R.A., and Simonetti, A. (2010) Constraints on the genesis of gold mineralization at the Homestake Gold Deposit, Black Hils, South Dakota from Re-Os sulfide geochronology. *Mineral. Deposita* **45**, 461-480.

Page, R. W., and Laing, W. P. (1992) Felsic metavolcanics rocks related to the Broken Hill Pb-Zn-Ag orebody, Australia: Geology, depositional age and timing of high-grade metamorphism. *Econ. Geol.* **87**, 2138-2168.

Page, R.W., Conor, C.H.H., Stevens, B.P.J., Gibson, G.M., Preiss, W.V., and Southgate, P.N. (2005a) Correlation of Olary and Broken Hill Domains, Curnamona Province: Possible Relationship to Mount Isa and Other North Australian Pb-Zn-Ag-Bearing Successions. *Econ. Geol*. **100**, 663-676.

Page, R.W., Stevens, B.P.J., and Gibson, G.M. (2005b) Geochronology of the sequence hosting the Broken Hill Pb-Zn-Ag orebody. *Econ. Geol*. **100**, 633-661.

Peucker-Ehrenbrink, B., and Jahn, B-M, (2001) Rhenium-osmium isotope systematic and platinum group element concentrations: Loess and the upper continental crust. *Geochem. Geophys. Geosyst*. **2**, 2001GC000172.

Phillips, G.N. (1980) Water activity changes across an amphibolites-granulite facies transition, Broken Hill, Australia. *Contrib. Mineral. Petrol.* **75**, 377-386.

543 Phillips, G.N., and Wall, V.J. (1981) Evaluation of prograde regional metamorphic conditions: their
544 implications for the heat source and water activity during metamorphism in the Willyama Complex.
545 *Bull. Mineral.* **104**, 801-810.
546 Plimer, I.R. (2006) Manganoan garnet rocks associated with the Broken Hill Pb-Zn-Ag orebody,
547 Australia. *Mineral. Petrol.* **88**, 443-478.
548 Pokrovski, G.S., Kara, S., and Roux, J. (2002) Stability and solubility of arsenopyrite, FeAsS, in crustal
549 fluids. *Geochim. Cosmochim. Acta* **66**, 2361-2378.
550 Prendergast, K., Stansfield, S., Williams, P.J. (1998) Syn-late tectonic metasomatism in Western A-lode,
551 Broken Hill. *Geol. Soc. Austral., Austral. Geol. Conv., Townsville, July 1998, Abs.***49**, 364.
552 Raič, S., Mogessie, A., Benko, Z., Molnar, F., Hauck, S., and Severson, M. (2014) Arsenic-enriched Cu-
553 Ni-PGE mineralization in Wetlegs, Duluth Complex, St Louis County, Minnesota, USA. *Eur. Geol.*
554 *Un. General Assembly* 2014, 27 April – 2 May 2014, Vienna, Austria, id. 3324.
555 Ruiz, J, and Mathur, R. (1999) Metallogenesis in continental margins: Re-Os evidence from porphyry
556 copper deposits in Chile. *Rev. Econ. Geol.* **12**, 59-72.
557 Saal, A.E., Rudnick, R.L., Ravizza, G.E., and Hart, S.R. (1998) Re-Os isotope evidence for the
558 composition, formation and age of the lower continental crust. *Nature* **397**, 58-61.
559 Schneider, J., Melcher, F., and Brauns, M. (2007) Concordant ages for the giant Kipushi base metal
560 deposit from direct Rb-Sr and Re-Os dating of sulfides. *Mineral. Deposita* **42**, 791-797.
561 Selby, D., Kelley, K.D., Hitzman, M.W., and Zieg, J. (2009) Re-Os sulfide (bornite, chalcopyrite, and
562 pyrite) systematics of the carbonate-hosted copper deposits at Ruby Creek, southern Brooks Range,
563 Alaska. *Econ. Geol.* **104**, 437-444.
564 Sharp, Z.D., Essene, E.J., Kelly, and W.C. (1985) A re-examination of the arsenopyrite geothermometer:
565 Pressure considerations and applications to natural assemblages. *Can. Mineral.* **23**, 517-534.

566 Smoliar, M.I., Walker, R.J., Morgan, J.W. (1996) Re-Os ages of Group IIA, IIIA, IVA and IVB iron
567 meteorites. *Science* **271**, 1099-1102.
568 Sparks, H.A., and Mavrogenes, J.A. (2003) Evidence in support of sulfide partial melting at Broken Hill,
569 Australia. *In* Mineral Exploration and Sustainable Development (D.G. Eliopoulos et al., eds.).
570 Millpress, Rotterdam, 1027-1029.
571 Spry, P. G. (1978) *The geochemistry of garnet-rich lithologies associated with the Broken Hill orebody,*
572 *N.S.W., Australia*. Unpublished M.S. thesis, University of Adelaide, Australia, 129 pp.
573 Spry, P. G., and Wonder J.D. (1989) Manganese-rich garnet rocks associated with the Broken Hill Pb-Zn-
574 Ag deposit, New South Wales, Australia. *Can. Mineral.* **27**, 275-292
575 Spry, P.G., Heimann, A., Messerly, J., and Houk, R.S. (2007) Discrimination of metamorphic and
576 metasomatic processes at the Broken Hill Pb-Zn-Ag deposit, Australia: Rare earth element signatures
577 of garnet-rich rocks. *Econ. Geol.* **102**, 471-494.
578 Stein, H.J., Sundblad, K., Markey, R.J., Morgan, J.W., and Motuza, G. (1998) Re-Os ages for Archean
579 molybdenite and pyrite, Kuittila-Kivisuo, Finland, and Proterozoic molybdenite, Kabeliai, Lithuania:
580 Testing the chronometer in a metamorphic and metasomatic setting. *Mineral. Deposita* **33**, 329-345.
581 Stevens, B.P.J. (1986) Post depositional history of the Willyama Supergroup in the Broken Hill Block,
582 New South Wales, Australia. *Austral. J. Earth Sci.* **33**, 73-98.
583 Sun, W., Bennett, V.C., Eggins, S.M., Kamenetsky, V.S., and Arculus, R.J. (2003) Enhanced mantle-to-
584 crust rhenium transfer in undegassed arc magmas. *Nature* **422**, 294-297.
585 Szymanski, J.T. (1979) The crystal structure of plararsite, Pt(As,S), and a comparison with sperrylite,
586 $PtAs_2$. *Can. Mineral.* **17**, 117-123.

587 Tomkins, A.G., and Mavrogenes, J.A. (2001) Redistribution of gold within arsenopyrite and loellingite
588 during pro- and retrograde metamorphism: Application to timing of mineralization. *Econ. Geol*. **96**,
589 525-534.
590 Tomkins, A.G., and Mavrogenes, J.A. (2002) Mobilization of gold as polymetallic melt during pelite
591 anatexis at the Challenger deposit, south Australia: A metamorphosed Archean gold deposit. *Econ.*
592 *Geol*. **97**, 1249-1271.
593 Tomkins, A.G., Frost, B.R., and Pattison, D.R.M. (2006) Arsenopyrite melting during metamorphism of
594 sulfide ore deposits. *Can. Mineral*. **44**, 1045-1062.
595 Tristá-Aguilera, D., Barra, F., Ruiz, J., Morata, D., Talavera-Mendoza, O., Kojima, S., and Ferraris, F.
596 (2006) Re-Os isotope systematics for the Lince-Estefanía deposit: Constraints on the timing and
597 source of copper mineralization in a stratabound copper deposit, Coastal Cordillera of northern Chile.
598 *Mineral. Deposita* **41**, 99-105.
599 Vaughan, J.P., and Stanton, R.L. (1984) Stratiform Pb-Zn mineralization in the Kuridala Formation and
600 Soldiers Cap Group, Mount Isa Block, NW Queensland Anonymous. *Conference Series – Australian*
601 *Institute of Mining and Metallurgy* **13**, 307-317.
602 Völkening, J., Walczyk, T., Heumann, K. (1991) Osmium isotopic ratio determination by negative thermal
603 ionization mass spectrometry. *Inter. J. Spectro. Ionic Phys.* **105**, 147-159.
604 Walker, R.J., Morgan, J.W., Naldrett, A.J., Li, C., and Fassett, J.D. (1991) Re-Os isotope systematic of
605 Ni-Cu sulfide ores, Sudbury Igneous Complex, Ontario: evidence for a major crustal component.
606 *Earth Planet. Sci. Lett*. **105**, 416-429.
607 Wright, J. V., Haydon, R. C., McConachy, G. W. (1987) Sedimentary model for the giant Broken Hill Pb-
608 Zn deposit. Australia. *Geology* **15**, 598-602.

609

Figures

Fig. 1 a. Location of the Broken Hill Zn-Pb-Ag deposit in New South Wales, Australia. **b.** Regional geology in the Broken Hill area (after Plimer, 2006). **c.** Geology of the Broken Hill deposit (after Plimer, 2006). **d.** Schematic reconstruction in map view of the spatial relationship between garnet rocks, quartz-bearing garnet rocks, gahnite-bearing garnet rocks and the different Zn- or Pb- ore lenses at the Broken Hill deposit (after Spry and Wonder, 1989).

Fig. 2 a. Polished slab of the sulfide-bearing spessartine-almandine sample utilised for Re-Os isotope geochemistry. Euhedral arsenopyrite is embedded in garnets. Anhedral arsenopyrite masses are also present. **b.** Polished thin section of this slab showing sulfide aggregates made of a core of löllingite and irregularly surrounded by arsenopyrite. Some grains of galena (white grains) are seen at the contact between löllingite and arsenopyrite. **c, d, e.** SEM-BSE images of arsenopyrite-löllingite mineralization. Two phases of galena (gn) precipitation are recorded. Tetrahedrite (tth) fills fractures in löllingite but not in arsenopyrite. In b and c, SEM-BSE images complemented by SEM-EDS analyses identified "invisible gold" in arsenopyrite (Point A at 2.0 wt.% Au, Point B at 4.8 wt% Au, see text for further details). **f.** Paragenetic sequence of the sample.

Fig. 3 Scanning electron microprobe images in backscattered mode (SEM-BSE) of mineral separates mounted in epoxy: **a.** +70 mesh, magnetic fraction at 2.2 amps, side slope at 2 º/forward slope at 10 º, **b.** 70–200 mesh, magnetic fraction at 1.7 amps, side slope at 15 º/forward slope at 10 º, **c.** +70 mesh, magnetic fraction at 1.7 amps, side slope at 15 º/forward slope at 10 º, **d.** +70 mesh, magnetic fraction at 2.2 amps, side slope at 2 º/forward slope at 10 º. Abbreviations: apy: arsenopyrite, gn: galena, löll: löllingite, Co-löll: cobaltian-löllingite (Co > 3wt%, SEM-EDX).

631 **Fig.4 a.** Re-Os isotope geochemistry data points for arsenopyrite, arsenopyrite ± löllingite, löllingite, and
632 löllingite ± arsenopyrite with error ellipses in the $^{187}Os/^{188}Os$ vs. $^{187}Re/^{188}Os$ space. **b.** Isochron regression
633 diagram of the 13 Re-Os data points of arsenopyrite and arsenopyrite ± löllingite. **c.** Isochron regression
634 diagram of the 5 Re-Os data points of löllingite and löllingite ± arsenopyrite.

635 # Tables

636 **Table 1** Elemental composition of löllingite and arsenopyrite as determined by qualitative SEM-EDX
637 analyses (error: ± 10%).

638 **Table 2** Mineral composition, magnetic susceptibility and Frantz fraction, and Re-Os isotopic data of
639 aliquots from arsenopyrite and löllingite in spessartine-almandine garnetite from the Broken Hill deposit.
640 +70 and 70-200 are the mesh size fractions, M: Magnetic at x, NM: non-magnetic at x, x = current in
641 amps, (y^{o}/z^{o}) = (side slope/forward slope).

642 **Table 3** Summary of metamorphic and thermal events in the Broken Hill Block, Curnamona Craton from
643 the late Paleoproterozoic to the Cambrian.

644 # Electronic Supplementary Material

645 **ESM 1.** SEM-EDX analyses of löllingite and arsenopyrite

Arsenopyrite

Analysis	S wt%	Fe wt%	Co wt%	Ni wt%	As wt%
ASP-1	15.34814	39.42061	2.987957	0.760265	41.48303
ASP-2	14.71611	31.93171	3.302426	0.918509	49.13125
ASP-3	15.38565	27.3567	3.81903	0.055266	53.38335
ASP-4	15.83976	29.99886	3.822591	0.049253	50.28954
ASP-5	15.88662	27.591	2.56343	0.171988	53.78696
ASP-6	16.19489	28.57611	2.914056	0.026317	52.28863
ASP-7	16.25506	29.73575	2.511198	0.091274	51.40672
ASP-8	16.26693	28.95398	2.578029	0.088183	52.11287
ASP-9	16.28922	29.02794	2.632546	0.147279	51.90301
ASP-10	16.44962	29.84402	2.826673	0.051159	50.82852
ASP-11	16.52589	29.66056	2.802993	0.02717	50.98339
ASP-12	16.61146	29.0412	2.203063	0.111597	52.03268
ASP-13	16.61972	29.56071	2.812177	0.040582	50.96681
ASP-14	16.64557	29.57659	2.140008	0.099073	51.53875
ASP-15	16.81037	28.6684	2.774725	0.023581	51.72293
ASP-16	16.83331	29.1658	1.718724	0.03653	52.24563
ASP-17	17.04628	30.19418	1.762478	n.d.	50.99706
ASP-18	17.06525	30.88247	1.675803	0.113215	50.26326
ASP-19	17.24658	30.34653	1.57359	0.050381	50.78291
ASP-20	17.25013	30.16522	3.32884	0.117362	49.13846
ASP-21	17.80119	32.44571	2.001477	0.104362	47.64726
ASP-22	17.58754	31.0154	1.852286	0.035545	49.50923
ASP-23	17.71382	29.81752	n.d.	n.d.	52.46866
ASP-24	17.74529	30.80848	n.d.	n.d.	51.44622
ASP-25	18.12601	31.00597	1.920603	0.106212	48.8412
ASP-26	17.96656	30.10853	1.784146	0	50.14077
ASP-27	18.01925	30.71091	n.d.	n.d.	51.26983
ASP-28	18.10489	31.18732	1.64285	n.d.	49.06493
ASP-29	18.22797	31.05131	2.002512	n.d.	48.71822
ASP-30	18.54335	30.14129	n.d.	n.d.	51.31536

Löllingite

Analysis	S wt%	Fe wt%	Co wt%	Ni wt%	As wt%
LOLL-1	0.814689	15.93468	4.676661	1.37703	77.19695
LOLL-2	0.871033	17.23238	4.569181	1.637343	75.69006
LOLL-3	0.871798	17.6505	4.886209	1.969954	74.62154
LOLL-4	0.878172	17.4051	4.931294	1.558914	75.22652
LOLL-5	0.897844	16.33508	5.192043	1.426127	76.14891
LOLL-6	0.964319	17.01019	5.139632	1.333733	75.55212
LOLL-7	0.97679	17.22186	5.373312	1.389941	75.0381
LOLL-8	1.024162	21.68702	4.200919	3.425245	69.66265
LOLL-9	1.114017	18.13948	4.759241	1.903244	74.08402
LOLL-10	1.205624	19.72281	3.305302	2.267154	73.49911
LOLL-11	1.205687	17.99259	4.492539	1.734019	74.57516
LOLL-12	1.226769	19.8915	3.086027	2.090567	73.70514

LOLL-13	1.241262	17.70948	4.103292	1.704083	75.24188
LOLL-14	1.269028	19.43346	3.389892	2.081368	73.82626
LOLL-15	1.284556	19.258	3.349359	2.265715	73.84237
LOLL-16	1.290174	18.38014	4.357797	2.00967	73.96221
LOLL-17	1.296789	19.24544	3.261305	2.190557	74.00591
LOLL-18	1.298523	20.33265	3.058541	2.207621	73.10266
LOLL-19	1.324842	20.51858	3.162012	2.14775	72.84681
LOLL-20	1.372534	18.42409	4.392293	1.780735	74.03035
LOLL-21	1.37327	19.42843	3.365471	2.299937	73.5329
LOLL-22	1.410314	20.54319	3.339693	2.298478	72.40833
LOLL-23	1.434068	17.76254	4.196858	1.877488	74.72905
LOLL-24	1.46553	19.02054	3.81405	2.004254	73.69562
LOLL-25	1.510775	19.9004	3.203086	2.324035	73.0617
LOLL-26	1.516597	19.88905	3.1716	2.293115	73.12963
LOLL-27	1.516801	19.6064	3.500531	2.264846	73.11142
LOLL-28	1.561934	17.93592	4.024124	1.736024	74.742
LOLL-29	1.598691	18.67714	4.375036	2.006676	73.34246
LOLL-30	1.633337	21.07243	3.552276	2.6545	71.08746
LOLL-31	1.665511	19.69736	3.099662	2.241955	73.29551

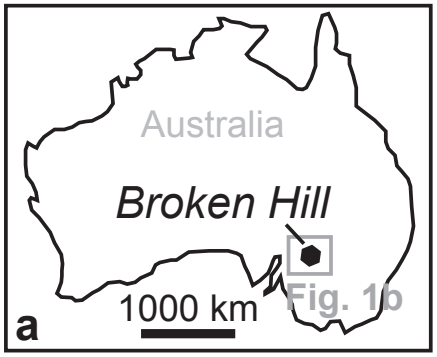

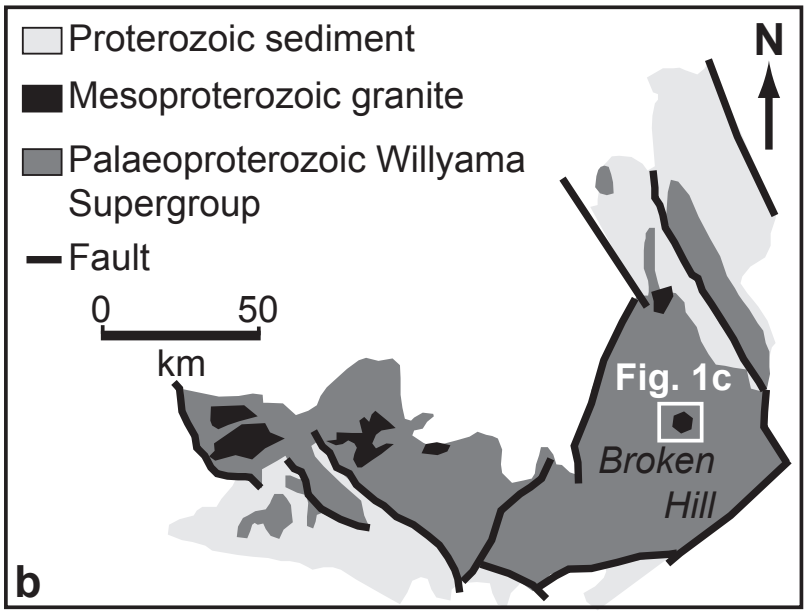

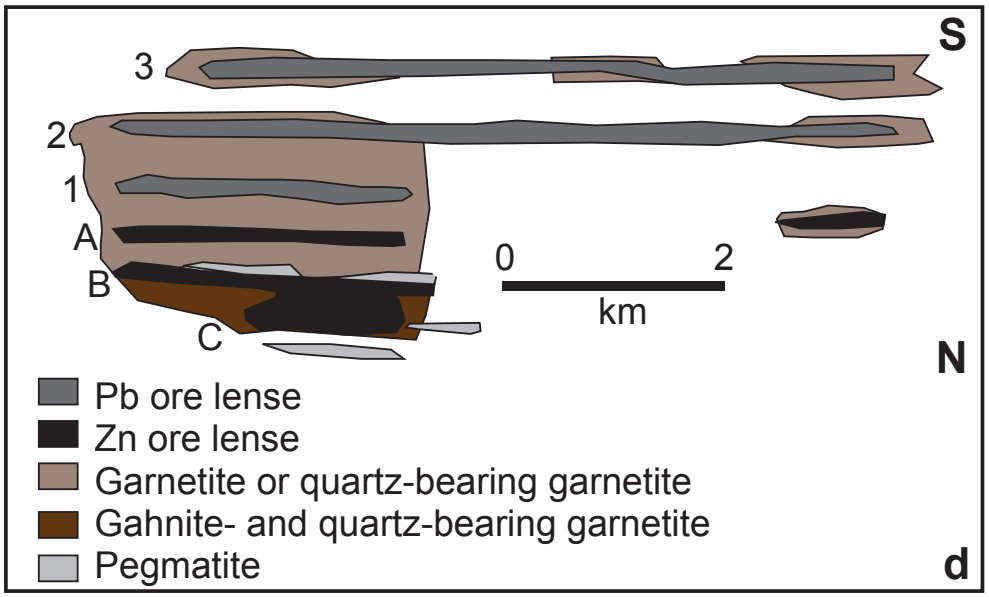

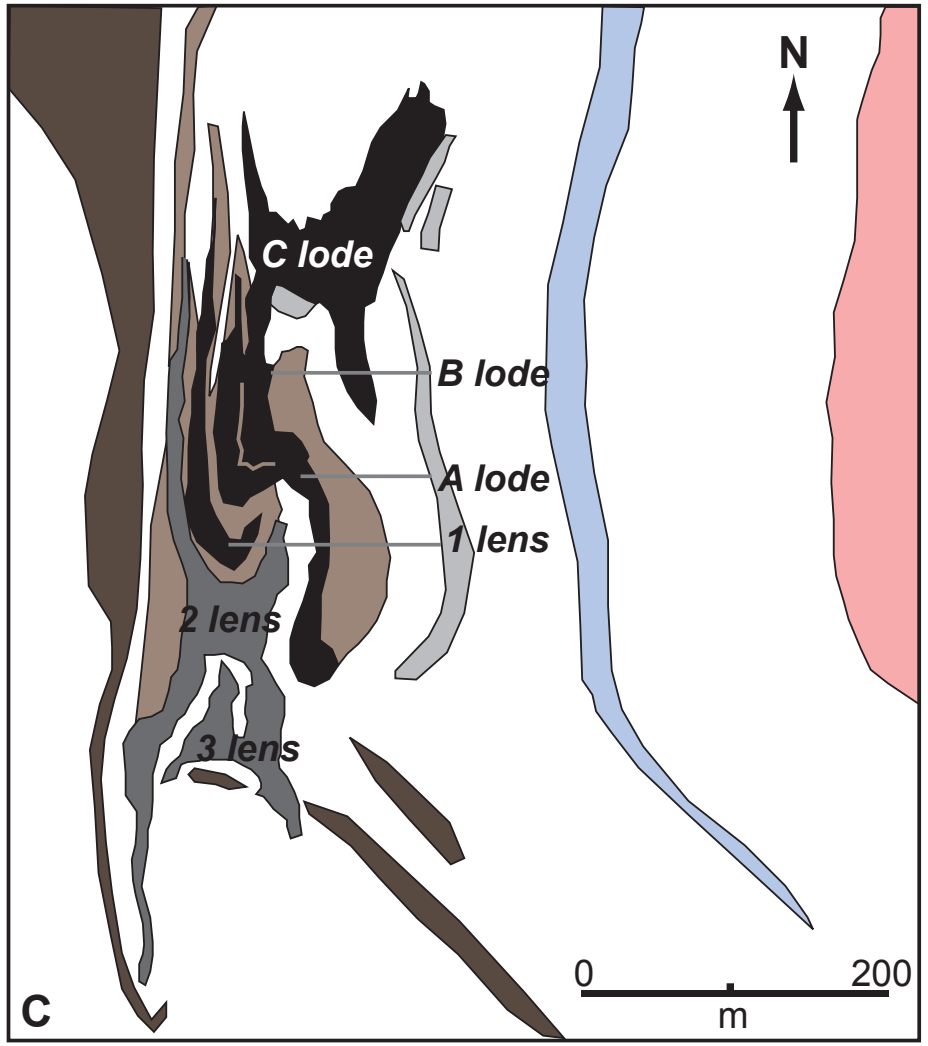

Legend

- Pb ore lense
- Zn ore lense
- Garnetite or quartz-bearing garnetite
- Garnet-plagioclase gneiss
- Pelitic, psammitic and psammopelitic metasediments
- Pegmatite
- Amphibolite
- Felsic gneiss

Figure 1

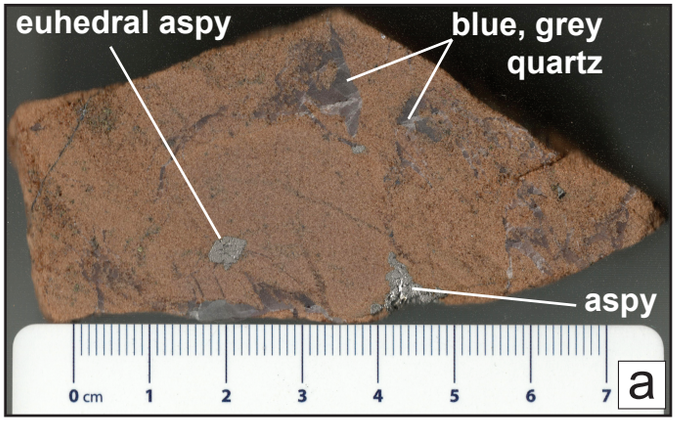
euhedral aspy
blue, grey quartz
aspy
0 cm 1 2 3 4 5 6 7
a

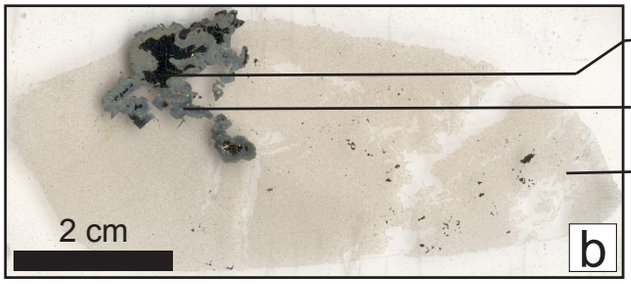
löllingite
arsenopyrite
garnet
2 cm
b

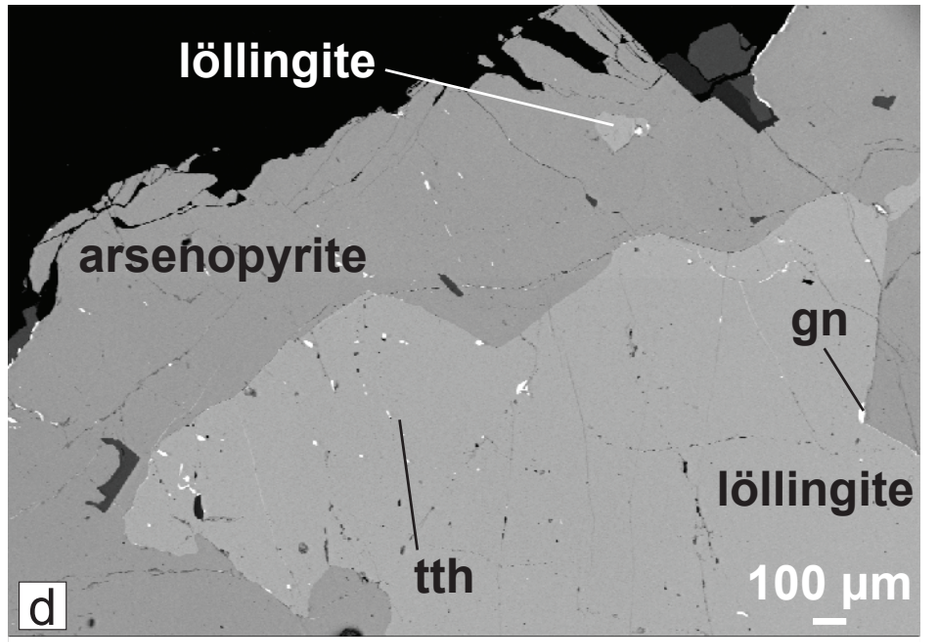
löllingite
arsenopyrite
gn
löllingite
tth
100 µm
d

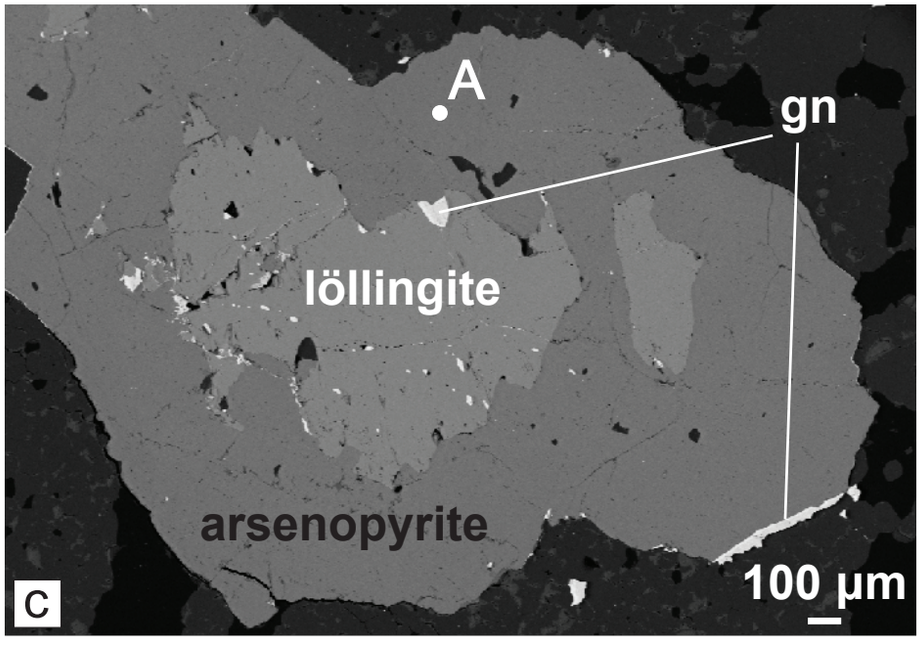
A
gn
löllingite
arsenopyrite
100 µm
c

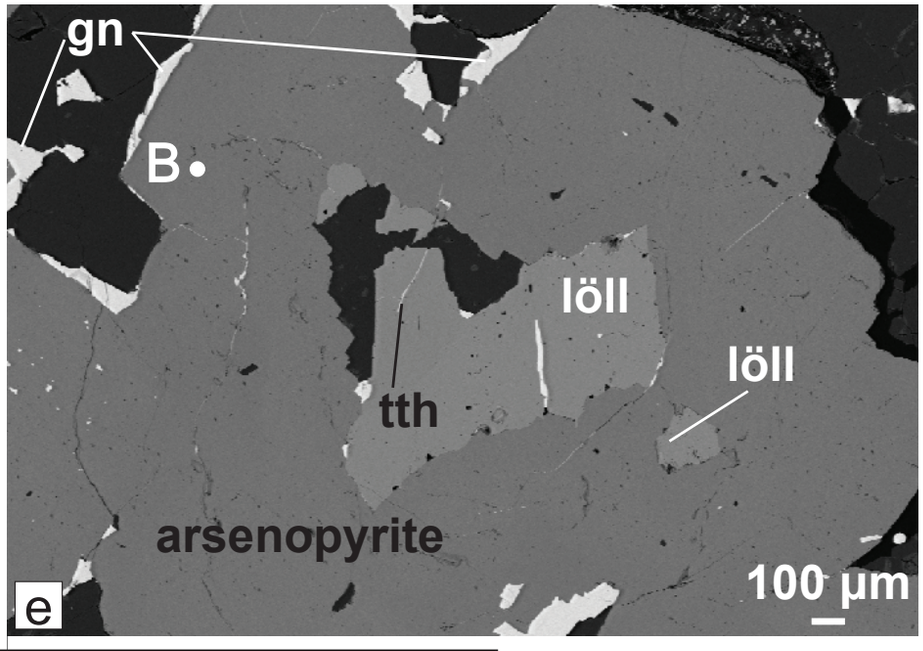
gn
B
löll
löll
tth
arsenopyrite
100 µm
e

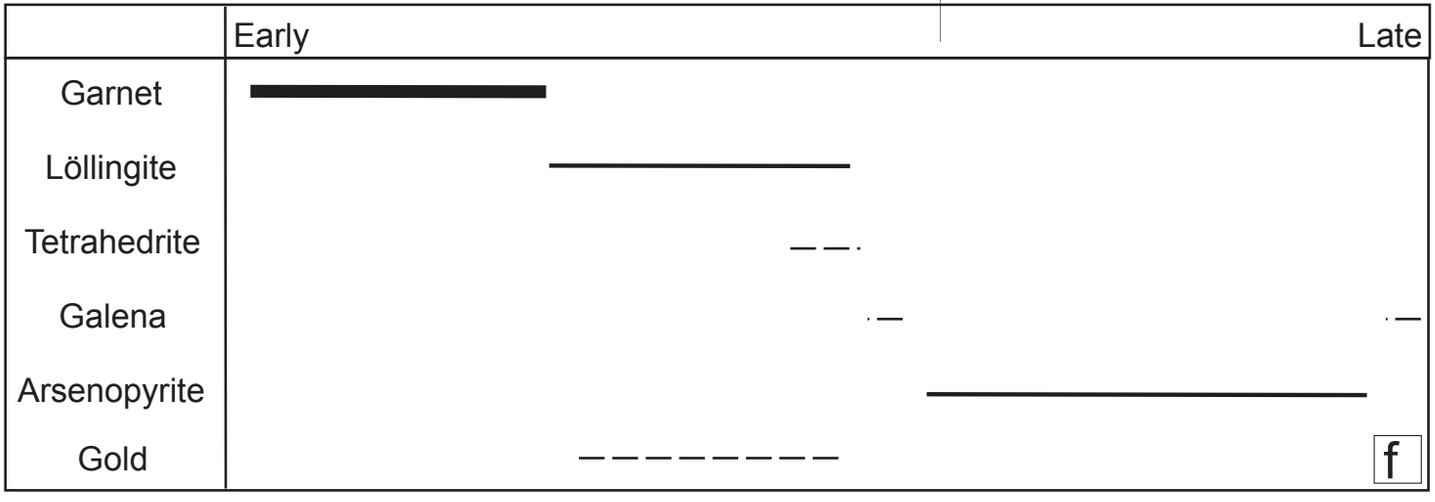
Early
Late
Garnet
Löllingite
Tetrahedrite
Galena
Arsenopyrite
Gold
f
Legend
< 5 vol %
> 5 and < 10 vol %
> 20 vol %

Fig. 2

Fig. 3

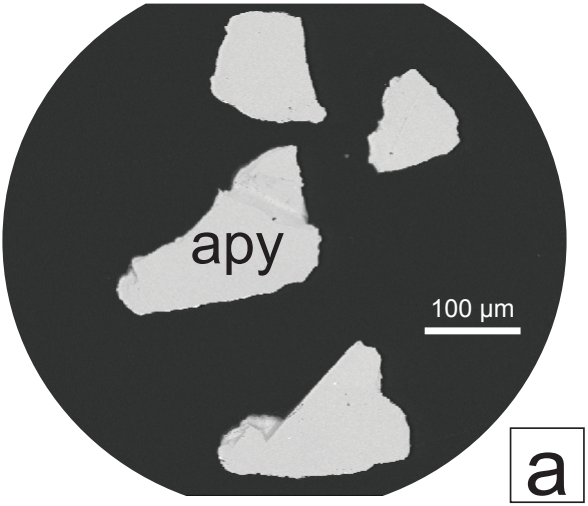

+70, NM 2.2 (2°/10°)

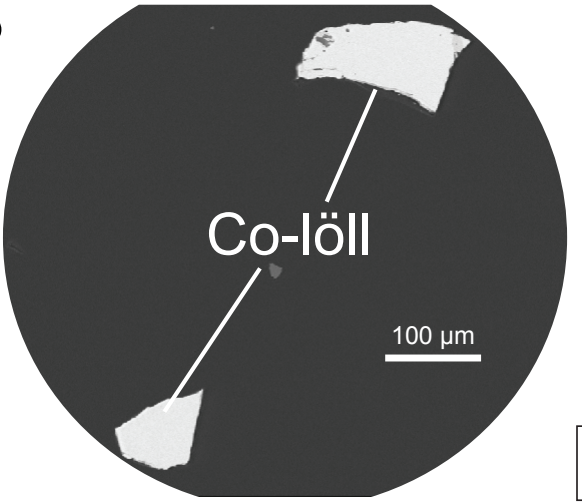

70-200, M 1.7 (15°/10°)

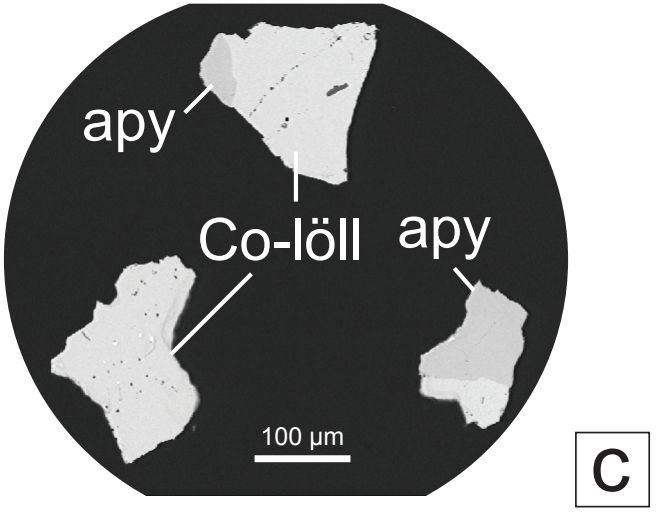

+70, M 1.7 (15°/10°)

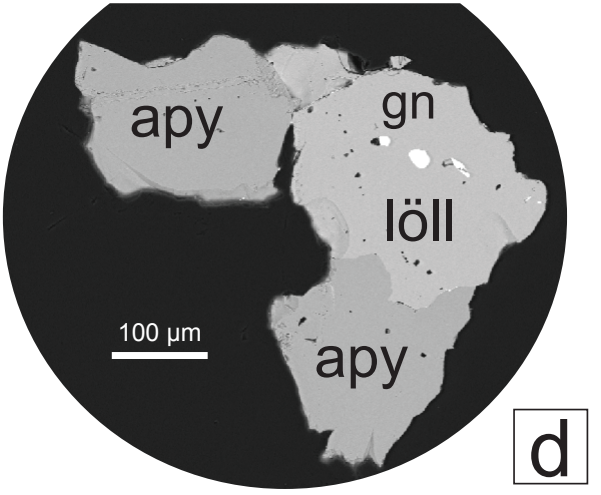

+70, M 2.2 (2°/10°)

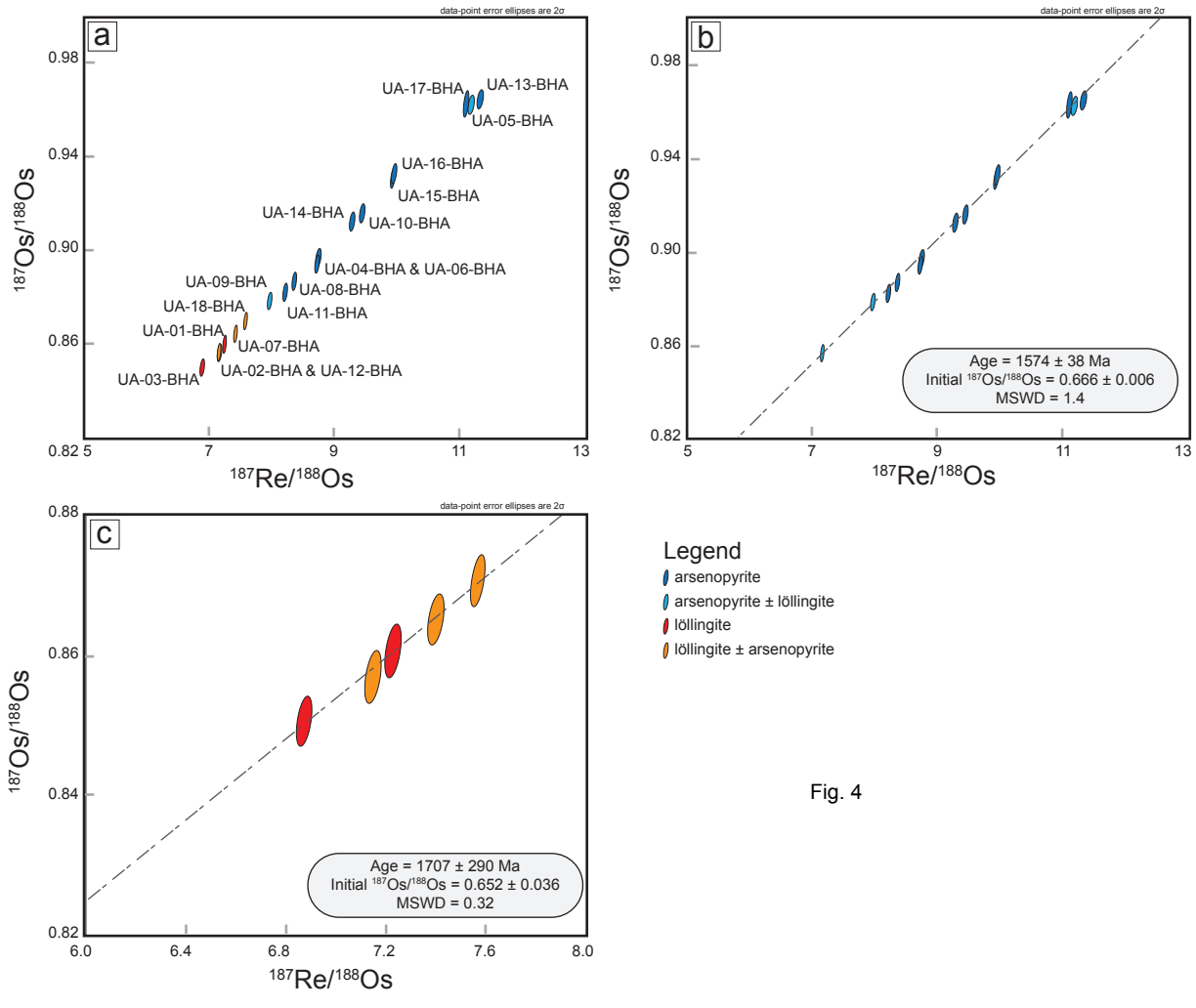
a
data-point error ellipses are 2σ
UA-17-BHA
UA-13-BHA
UA-05-BHA
UA-16-BHA
UA-15-BHA
UA-14-BHA
UA-10-BHA
UA-04-BHA & UA-06-BHA
UA-09-BHA
UA-08-BHA
UA-18-BHA
UA-11-BHA
UA-01-BHA
UA-07-BHA
UA-03-BHA
UA-02-BHA & UA-12-BHA
187Os/188Os
187Re/188Os
b
data-point error ellipses are 2σ
Age = 1574 ± 38 Ma
Initial 187Os/188Os = 0.666 ± 0.006
MSWD = 1.4
187Os/188Os
187Re/188Os
c
data-point error ellipses are 2σ
Age = 1707 ± 290 Ma
Initial 187Os/188Os = 0.652 ± 0.036
MSWD = 0.32
187Os/188Os
187Re/188Os
Legend
arsenopyrite
arsenopyrite ± löllingite
löllingite
löllingite ± arsenopyrite

Fig. 4

Löllingite (n = 31)	**S wt.%**	**Fe wt.%**	**Co wt.%**	**Ni wt.%**	**As wt.%**
average	1.3	18.8	4.0	2.0	74.0
standard deviation	0.3	1.4	0.7	0.4	1.4

Arsenopyrite (n = 30)	**S wt.%**	**Fe wt.%**	**Co wt.%**	**Ni wt.%**	**As wt.%**
average	16.9	30.3	2.1	0.1	50.6
standard deviation	0.9	2.0	1.0	0.2	2.2

Table 1

Sample	Frantz magnetic fraction	Mineralogy (XRD data and SEM images)	Weight (mg)	Re (ppb)	± 2σ	Total Os (ppt)	± 2σ	$^{187}Re/^{188}Os$	± 2σ	$^{187}Os/^{188}Os$	± 2σ	rho	% Re blank	$\%^{187}Os$ blank	$\%^{188}Os$ blank
UA-05-BHA	+70, mag 2.2, 2/10	arsenopyrite ± löllingite	20.86	133.6	0.5	63919	181	11.17	0.04	0.9628	0.0034	0.454	0.02	0.009	0.030
UA-09-BHA	+70, mag 2.2, 2/10	arsenopyrite ± löllingite	27.49	382.5	1.4	254782	701	7.94	0.03	0.8791	0.0031	0.459	0.01	0.002	0.006
UA-12-BHA	+70, mag 2.2, 2/10	arsenopyrite ± löllingite	24.81	142.9	0.5	105605	287	7.14	0.03	0.8574	0.0030	0.461	0.02	0.005	0.015
UA-06-BHA	+70, non-mag 2.2, 2/10	arsenopyrite	20.31	320.2	1.2	194463	537	8.73	0.03	0.8977	0.0032	0.461	0.01	0.003	0.010
UA-10-BHA	+70, non-mag 2.2, 2/10	arsenopyrite	20.85	209.0	0.8	117826	332	9.43	0.03	0.9165	0.0033	0.451	0.02	0.005	0.016
UA-11-BHA	+70, non-mag 2.2, 2/10	arsenopyrite	20.16	239.4	0.9	151940	415	8.34	0.03	0.8875	0.0031	0.458	0.01	0.004	0.013
UA-13-BHA	+70, non-mag 2.2, 2/10	arsenopyrite	36.20	246.4	0.9	116388	329	11.32	0.04	0.9654	0.0034	0.460	0.01	0.003	0.009
UA-14-BHA	+70, non-mag 2.2, 2/10	arsenopyrite	32.00	121.3	0.4	69525	198	9.27	0.03	0.9130	0.0034	0.459	0.02	0.005	0.018
UA-15-BHA	+70, non-mag 2.2, 2/10	arsenopyrite	20.60	159.1	0.5	85410	240	9.92	0.03	0.9315	0.0033	0.539	0.07	0.004	0.005
UA-16-BHA	+70, non-mag 2.2, 2/10	arsenopyrite	12.92	140.3	0.4	75147	217	9.94	0.03	0.9334	0.0035	0.529	0.13	0.007	0.008
UA-17-BHA	+70, non-mag 2.2, 2/10	arsenopyrite	16.83	146.8	0.5	70767	237	11.09	0.04	0.9633	0.0045	0.540	0.09	0.006	0.007
UA-04-BHA	70-200, non-mag 2.2, 2/10	arsenopyrite	20.91	174.5	0.6	106192	296	8.71	0.03	0.8949	0.0032	0.458	0.02	0.006	0.018
UA-08-BHA	70-200, non-mag 2.2, 2/10	arsenopyrite	21.41	225.1	0.8	145315	397	8.20	0.03	0.8828	0.0031	0.460	0.01	0.004	0.013
UA-01-BHA	70-200, mag 1.7, 15/10	löllingite	10.86	473.4	1.7	345733	950	7.23	0.03	0.8607	0.0031	0.464	0.01	0.003	0.010
UA-03-BHA	70-200, mag 1.7, 15/10	löllingite	14.33	397.0	1.4	304605	809	6.87	0.03	0.8506	0.0029	0.459	0.01	0.003	0.009
UA-18-BHA	+70, mag 1.7, 15/10	löllingite ± arsenopyrite	14.46	318.5	1.0	222444	603	7.57	0.02	0.8707	0.0030	0.539	0.05	0.002	0.002
UA-02-BHA	+70, mag 1.7, 15/10	löllingite ± arsenopyrite	12.69	449.8	1.6	332046	907	7.15	0.03	0.8570	0.0031	0.459	0.01	0.003	0.009
UA-07-BHA	+70, mag 1.7, 15/10	löllingite ± arsenopyrite	13.46	392.1	1.4	279816	753	7.40	0.03	0.8651	0.0030	0.461	0.01	0.003	0.010

Table 2

Age (Ma)	Orogeny	Metamorphic event/grade	T(ºC), P (kbar)	Mineral (Method)	Reference
1657 ± 8	Static?	lower amphibolite facies	<550?, <3?	Monazite (U-Pb)	Holdaway (1971); McFarlane and Frost (2009)
1630 ± 6	Olarian orogeny	upper amphibolite facies (prograde)	>650, 3–4	Monazite (U-Pb)	Holdaway (1971); McFarlane and Frost (2009)
1602 ± 9	Olarian orogeny	granulite facies (peak)	~800, 5–6	Monazite (U-Pb)	Holdaway (1971); McFarlane and Frost (2009)
1590–1575	Olarian orogeny	(retrograde)	< 650, ~5	Monazite (U-Pb)	Holdaway (1971); McFarlane and Frost (2009)
1660–1570	Olarian orogeny	prograde to retrogade	Cooling, below 500ºC after 1500 Ma, rate ~3ºC/Ma	hornblende, plagioclase, clinopyroxene (^{40}Ar-^{39}Ar)	Harrison and McDougall (1981)
1574 ± 38	Late Olarian orogeny?	(retrograde)	<550 for stability field of arsenopyrite of 400–500ºC, ~5	Arsenopyrite (Re-Os)	this study
517–497	Delamerian orogeny	garnet-staurolite-biotite-muscovite-chlorite-quartz	530–600, ~5 (located in shear zones)	Monazite, garnet (U-Pb, Sm-Nd)	Dutch et al. (2005)
520 ± 40	Delamerian orogeny		~350	Biotite (Rb-Sr)	Harrison and McDougall (1981)

Table 3